

1
2
3
4
5
6

7
8
9
10

11
12
13
14
15
16
17
18
19
20
21
22
23
24
25
26

Original Research Article
**MHD Free Convection, Heat and Mass Transfer
Chemical Reaction, Radiation and Heat Source
or Sink over a Rotating Inclined Permeable
Plate Variable Reactive Index**

ABSTRACT

MHD free convection, heat and mass transfer flow over a rotating inclined permeable plate with the influence of magnetic field, thermal radiation and chemical reaction of various order has been investigated numerically. The governing boundary-layer equations are formulated and transformed into a set of similarity equations with the help of similarity variables derived by lie group transformation. The governing equations are solved numerically using the Nactsheim-Swigert Shooting iteration technique together with the Runge-Kutta six order iteration schemes. The simulation results are presented graphically to illustrate influence of magnetic parameter (M), porosity parameter (γ), rotational parameter (R'), Grashof number (G_r), modified Grashof number (G_m), thermal conductivity parameter (T_c), Prandtl number (P_r), radiation parameter (R), heat source parameter (Q), Eckert number (E_c), Schmidt number (S_c), reaction parameter (λ) and order of chemical reaction (n) on the all fluid velocity components, temperature and concentration distribution as well as Skin-friction coefficient, Nusselt and Sherwood number at the plate.

Keywords: MHD; Inclined permeable plate; Thermal radiation; Chemical reaction;

NOMENCLATURE

B_0	Constant magnetic flux density
c	Constant depends on the properties of the fluid
C	Concentration of the fluid
C_p	Specific heat at constant pressure
D_m	Mass diffusivity
f'	Dimensionless primary velocity
g	Acceleration due to gravity
g_0	Dimensionless secondary velocity
k	Thermal conductivity
k_∞	Undisturbed thermal conductivity
k_0	Reaction rate

27	K	Permeability of the porous medium
28	n	Order of chemical reaction
29	P	Pressure distribution in the boundary layer
30	q_r	Radiative heat flux in the y direction
31	Q_T	Heat generation
32	Q_0	Heat source
33	t	Time
34	T	Fluid temperature
35	U	Uniform velocity
36	u, v	Velocity components along x and y axes respectively
37	x'	Dimensionless axial distance along x axis
38	Dimensionless parameters	
39	E_c	Eckert number
40	R'	Rotational parameter
41	G_r	Grashof number
42	G_m	Modified Grashof number
43	M	Magnetic parameter
44	P_r	Prandtl number
45	Q	Heat source parameter
46	R	Radiation parameter
47	S_c	Schmidt number
48	T_c	Thermal conductivity parameter
49	γ	Permeability of the porous medium
50	λ	Reaction parameter

51

52 **Greek Symbols**

53	ν	Kinematic viscosity of the fluid
54	μ	Dynamic viscosity of the fluid
55	σ	Electrical conductivity
56	σ_0	Constant electrical conductivity
57	σ_s	Stefan-Boltzmann constant
58	ρ	Density of the fluid

59	α	Thermal diffusivity
60	$\alpha_1 - \alpha_6$	Arbitrary real number
61	β	Inclination angle
62	β_T	Thermal expansion coefficient
63	β_C	Concentration expansion coefficient
64	κ^*	Mean absorption coefficient
65	ε	Parameter of the group
66	ψ	Stream function
67	η	Similarity variable
68	θ	Dimensionless temperature
69	ϕ	Dimensionless concentration
70	Ω	Angular velocity of the plate
71	Subscripts	
72	w	Condition of the wall
73	∞	Condition of the free steam

74
75
76

1. INTRODUCTION

77 Coupled heat and mass transfer problems in the presence of chemical reactions are of
78 importance in many processes and have, therefore, received considerable amount of
79 attention of researchers in recent years. Chemical reactions can occur in processes such as
80 drying, distribution of temperature and moisture over agricultural fields and groves of fruit
81 trees, damage of crops due to freezing, evaporation at the surface of a water body, energy
82 transfer in a wet cooling tower and flow in a desert cooler. Chemical reactions are classified
83 as either homogeneous or heterogeneous processes. A homogeneous reaction is one that
84 occurs uniformly throughout a given phase. On the other hand, a heterogeneous reaction
85 takes a restricted area or within the boundary of a phase. Analysis of the transport
86 processes and their interaction with chemical reactions is quite difficult and closely related to
87 fluid dynamics. Chemical reaction effects on heat and mass transfer has been analyzed by
88 many researchers over various geometries with various boundary conditions in porous and
89 nonporous media. Symmetry groups or simply symmetries are invariant transformations that
90 do not alter the structural form of the equation under investigation which is described by
91 Bluman and Kumei [1]. MHD boundary layer equations for power law fluids with variable
92 electric conductivity is studied by Helmy [2]. In the case of a scaling group of
93 transformations, the group-invariant solutions are nothing but the well known similarity
94 solutions which is studied by Pakdemirli and Yurusoy [3]. Symmetry groups and similarity
95 solutions for free convective boundary-layer problem was studied by Kalpakides and
96 Balassas [4]. Makinde [5] investigated the effect of free convection flow with thermal
97 radiation and mass transfer past moving vertical porous plate. Seddeek and Salem [6]
98 investigated the Laminar mixed convection adjacent to vertical continuously stretching sheet
99 with variable viscosity and variable thermal diffusivity. Ibrahim, Elaiw and Bakr [7] studied the
100 effect of the chemical reaction and radiation absorption on the unsteady MHD free
101 convection flow past a semi infinite vertical permeable moving plate with heat source and

suction. El-Kabeir, El-Hakiem and Rashad [8] studied Lie group analysis of unsteady MHD three dimensional dimensional by natural convection from an inclined stretching surface saturated porous medium. Rajeswari, Jothiram and Nelson [9] studied the effect of chemical reaction, heat and mass transfer on nonlinear MHD boundary layer flow through a vertical porous surface in the presence of suction. Chandrakala [10] investigated chemical reaction effects on MHD flow past an impulsively started semi-infinite vertical plate. Joneidi, Domairry and Babaelahi [11] studied analytical treatment of MHD free convective flow and mass transfer over a stretching sheet with chemical reaction. Muhaimin, Kandasamy and Hashim [12] studied the effect of chemical reaction, heat and mass transfer on nonlinear boundary layer past a porous shrinking sheet in the presence of suction. Rahman and Salahuddin [13] studied hydromagnetic heat and mass transfer flow over an inclined heated surface with variable viscosity and electric conductivity. As per standard text and works of previous researchers, the radiative flow of an electrically conducting fluid and heat and mass transfer situation arises in many practical applications such as in electrical power generation, astrophysical flows, solar power technology, space vehicle re-entry, nuclear reactors.

The objective of this study is to present a similarity analysis of boundary layer flow past a rotating inclined permeable plate with the influence of magnetic field, thermal radiation, thermal conductivity and chemical reaction of various orders.

2. MATHEMATICAL MODEL OF THE FLOW AND GOVERNING EQUATIONS

Steady two dimensional MHD heat and mass transfer flow with chemical reaction and radiation over an inclined permeable plate $y=0$ in a rotating system under the influence of transversely applied magnetic field is considered. The x -axis is taken in the upward direction and y -axis is normal to it. Again the plate is inclined at an angle β with the x -axis. The flow takes place at $y \geq 0$, where y is the coordinate measured normal to the x -axis. Initially we consider the plate as well as the fluid is at rest with the same velocity $U (=U_\infty)$, temperature $T(=T_\infty)$ and concentration $C(=C_\infty)$. Also it is assumed that the fluid and plate is at rest after that the whole system is allowed to rotate with a constant angular velocity $R=(0,-\Omega,0)$ about the y -axis and then the temperature and species concentration of the plate are raised to $T_w(>T_\infty)$ and $C_w(>C_\infty)$ respectively, which are thereafter maintained constant, where T_w and C_w is the temperature and concentration respectively at wall and T_∞ and C_∞ is the temperature and concentration respectively far away from the plate.

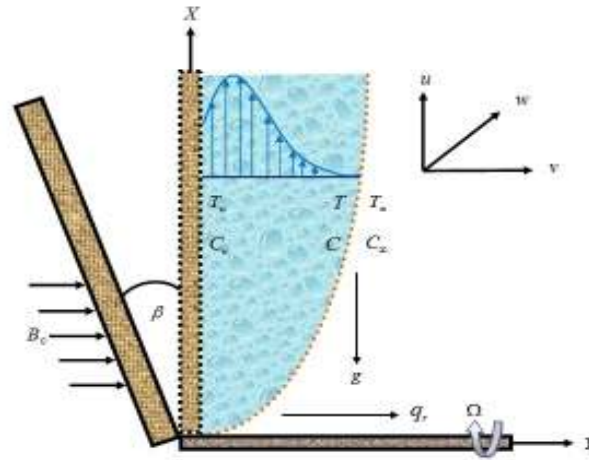


Fig. 1. Physical configuration of the flow

138 The electrical conductivity is assumed to vary with the velocity of the fluid and have the form
139 [2],

140 $\sigma = \sigma_0 u$, σ_0 is the constant electrical conductivity.

141 The applied magnetic field strength is considered, as follows [13]

$$142 \quad B(x) = \frac{B_0}{\sqrt{x}}$$

143 The temperature dependent thermal conductivity is assumed to vary linearly, as follows [6]

$$144 \quad k(T) = k_\infty [1 + c(T - T_\infty)]$$

145 Where k_∞ is the undisturbed thermal conductivity and c is the constant depending on the
146 properties of the fluid.

147 The governing equations for the continuity, momentum, energy and concentration in laminar
148 MHD incompressible boundary-layer flow is presented follows

$$149 \quad \frac{\partial u}{\partial x} + \frac{\partial v}{\partial y} = 0 \quad (1)$$

$$150 \quad u \frac{\partial u}{\partial x} + v \frac{\partial u}{\partial y} = v \frac{\partial^2 u}{\partial y^2} + 2\Omega w - \frac{v}{K} u - \frac{\sigma_0 B_0^2 u^2}{\rho x} + g\beta_T (T - T_\infty) \cos\beta + g\beta_C (C - C_\infty) \cos\beta \quad (2)$$

$$151 \quad u \frac{\partial w}{\partial x} + v \frac{\partial w}{\partial y} = v \frac{\partial^2 w}{\partial y^2} - 2\Omega u - \frac{v}{K} w - \frac{\sigma_0 B_0^2 u w}{\rho x} \quad (3)$$

$$152 \quad u \frac{\partial T}{\partial x} + v \frac{\partial T}{\partial y} = \frac{1}{\rho C_p} \frac{\partial}{\partial y} \left[k(T) \frac{\partial T}{\partial y} \right] + \frac{Q_0 (T - T_\infty)}{\rho C_p} - \frac{\alpha}{k_\infty} \left(\frac{\partial q_r}{\partial y} \right) + \frac{v}{C_p} \left(\frac{\partial u}{\partial y} \right)^2 \quad (4)$$

$$153 \quad u \frac{\partial C}{\partial x} + v \frac{\partial C}{\partial y} = D_m \frac{\partial^2 C}{\partial y^2} - k_0 (C - C_\infty)^n \quad (5)$$

154 and the boundary conditions for the model is

$$155 \quad \left. \begin{aligned} u = U, v = 0, w = 0, T = T_w, C = C_w \quad \text{at } y = 0 \\ u \rightarrow 0, w \rightarrow 0, T \rightarrow T_\infty, C \rightarrow C_\infty \quad \text{as } y \rightarrow \infty \end{aligned} \right\} \quad (6)$$

156 where, U is the uniform velocity, β is the inclination angle of the plate with x-axis, C_p is the
157 specific heat at constant pressure, $k(T)$ is the temperature dependent thermal conductivity,
158 Q_0 is the heat source, D_m is the mass diffusivity, k_0 is the reaction rate, $k_0 > 0$ for destructive
159 reaction, $k_0 = 0$ for no reaction and $k_0 < 0$ for generative reaction, n (integer) is the order of
160 chemical reaction, q_r is the chemical reaction parameter, T_w and C_w is the temperature and
161 concentration respectively at wall and T_∞ and C_∞ is the temperature and concentration
162 respectively far away from the plate.

163

164 2.1 METHOD OF SOLUTION

165

166 Introducing the following dimensionless variables

$$167 \quad x' = \frac{xU}{v}, y' = \frac{yU}{v}, u' = \frac{u}{U}, v' = \frac{v}{U}, w' = \frac{w}{U}, \theta = \frac{T - T_\infty}{T_w - T_\infty} \quad \text{and} \quad \phi = \frac{C - C_\infty}{C_w - C_\infty}$$

168 the following equations are obtained,

$$169 \quad u = U u', v = U v', w = U w', T = T_\infty + (T_w - T_\infty) \theta \quad \text{and} \quad C = C_\infty + (C_w - C_\infty) \phi \quad (7)$$

170 Now, by using equation (7), the equations (1), (2), (3), (4) and (5) are transformed to

$$171 \quad \frac{\partial u'}{\partial x'} + \frac{\partial v'}{\partial y'} = 0 \quad (8)$$

$$u' \frac{\partial u'}{\partial x'} + v' \frac{\partial u'}{\partial y'} = \frac{\partial^2 u'}{\partial y'^2} + 2R'w' - \gamma u' - \frac{Mu'^2}{x'} + G_r \theta \cos \beta + G_m \phi \cos \beta \quad (9)$$

$$u' \frac{\partial w'}{\partial x'} + v' \frac{\partial w'}{\partial y'} = \frac{\partial^2 w'}{\partial y'^2} - 2R'u' - \gamma w' - \frac{Mu'w'}{x'} \quad (10)$$

$$u' \frac{\partial \theta}{\partial x'} + v' \frac{\partial \theta}{\partial y'} - \frac{1}{P_r} \left[(1 + T_c \theta + R) \frac{\partial^2 \theta}{\partial y'^2} + T_c \left(\frac{\partial \theta}{\partial y'} \right)^2 \right] - Q\theta - E_c \left(\frac{\partial u}{\partial y} \right)^2 = 0 \quad (11)$$

$$u' \frac{\partial \phi}{\partial x'} + v' \frac{\partial \phi}{\partial y'} - \frac{1}{S_c} \frac{\partial^2 \phi}{\partial y'^2} + \lambda \phi^n = 0 \quad (12)$$

using equation (7), the boundary condition (6) becomes,

$$\left. \begin{aligned} u' = 1, v' = 0, w' = 0, \theta = 1, \phi = 1 \text{ at } y' = 0 \\ u' \rightarrow 0, w' \rightarrow 0, \theta \rightarrow 0, \phi \rightarrow 0 \text{ as } y' \rightarrow \infty \end{aligned} \right\} \quad (13)$$

where,

$$R' = \frac{\Omega v}{U^2}, \gamma = \frac{v^2}{KU^2}, M = \frac{\sigma_0 B_0^2}{\rho}, G_r = \frac{g \beta_T (T_w - T_\infty) v}{U^3}, G_m = \frac{g \beta_c (C_w - C_\infty) v}{U^3}, T_c = c(T_w - T_\infty),$$

$$R = \frac{16\sigma_s T_\infty^3}{3\kappa^* k_\infty}, P_r = \frac{v}{\alpha}, Q = \frac{Q_0 v}{\rho C_p U^2}, E_c = \frac{U^2}{C_p (T_w - T_\infty)}, S_c = \frac{v}{D_m} \text{ and } \lambda = \frac{k_0 (C_w - C_\infty)^{n-1} v}{U^2}$$

In order to deal with the problem, we introduce the stream function ψ (since the flow is incompressible) defined by

$$u' = \frac{\partial \psi}{\partial y'}, v' = -\frac{\partial \psi}{\partial x'} \quad (14)$$

The mathematical significance of using equation (14) is that the continuity equation (8) is satisfied automatically.

by equation (14), equations (9), (10), (11) and (12) transformed as follows,

$$\frac{\partial \psi}{\partial y'} \frac{\partial^2 \psi}{\partial x' \partial y'} - \frac{\partial \psi}{\partial x'} \frac{\partial^2 \psi}{\partial y'^2} - \frac{\partial^3 \psi}{\partial y'^3} - 2R'w' + \gamma \frac{\partial \psi}{\partial y'} + \frac{M}{x'} \left(\frac{\partial \psi}{\partial y'} \right)^2 - G_r \theta \cos \beta - G_m \phi \cos \beta = 0 \quad (15)$$

$$\frac{\partial \psi}{\partial y'} \frac{\partial w'}{\partial x'} - \frac{\partial \psi}{\partial x'} \frac{\partial w'}{\partial y'} - \frac{\partial^2 w'}{\partial y'^2} + 2R' \frac{\partial \psi}{\partial y'} + \gamma w' + \frac{M}{x'} \frac{\partial \psi}{\partial y'} w' = 0 \quad (16)$$

$$\frac{\partial \psi}{\partial y'} \frac{\partial \theta}{\partial x'} - \frac{\partial \psi}{\partial x'} \frac{\partial \theta}{\partial y'} - \frac{1}{P_r} \left[(1 + T_c \theta + R) \frac{\partial^2 \theta}{\partial y'^2} + T_c \left(\frac{\partial \theta}{\partial y'} \right)^2 \right] - Q\theta - E_c \left(\frac{\partial^2 \psi}{\partial y'^2} \right)^2 = 0 \quad (17)$$

$$\frac{\partial \psi}{\partial y'} \frac{\partial \phi}{\partial x'} - \frac{\partial \psi}{\partial x'} \frac{\partial \phi}{\partial y'} - \frac{1}{S_c} \frac{\partial^2 \phi}{\partial y'^2} + \lambda \phi^n = 0 \quad (18)$$

and the boundary conditions (13) become,

$$\left. \begin{aligned} \frac{\partial \psi}{\partial y'} = 1, \frac{\partial \psi}{\partial x'} = 0, w' = 0, \theta = 1, \phi = 1 \text{ at } y' = 0 \\ \frac{\partial \psi}{\partial y'} \rightarrow 0, w' \rightarrow 0, \theta \rightarrow 0, \phi \rightarrow 0 \text{ as } y' \rightarrow \infty \end{aligned} \right\} \quad (19)$$

Finding the similarity solution of the equations (15) to (18) is equivalent to determining the invariant solutions of these equations under a particular continuous one parameter group. Introducing the simplified form of Lie-group transformations [8] namely, the scaling group of transformations

$$G_1: x^* = x'e^{\varepsilon\alpha_1}, y^* = y'e^{\varepsilon\alpha_2}, \psi^* = \psi e^{\varepsilon\alpha_3}, w^* = w'e^{\varepsilon\alpha_4}, \theta^* = \theta e^{\varepsilon\alpha_5} \text{ and } \varphi^* = \varphi e^{\varepsilon\alpha_6} \quad (20)$$

Here, $\varepsilon(\neq 0)$ is the parameter of the group and α_i 's are arbitrary real numbers whose interrelationship will be determined by our analysis. Equations (20) may be considered as a point transformation which transforms the coordinates $(x', y', \psi, w', \theta, \varphi)$ to the coordinates $(x^*, y^*, \psi^*, w^*, \theta^*, \varphi^*)$.

The system will remain invariant under the group transformation G_1 , so the following relations among the exponents are obtained from equations (15) to (18),

$$\left. \begin{aligned} \alpha_1 + 2\alpha_2 - 2\alpha_3 &= 3\alpha_2 - \alpha_3 = -\alpha_4 = \alpha_2 - \alpha_3 = -\alpha_5 = -\alpha_6 \\ \alpha_1 + \alpha_2 - \alpha_3 - \alpha_4 &= 2\alpha_2 - \alpha_4 = \alpha_2 - \alpha_3 = -\alpha_4 \\ \alpha_1 + \alpha_2 - \alpha_3 - \alpha_5 &= 2\alpha_2 - \alpha_5 = 2\alpha_2 - 2\alpha_5 = 4\alpha_2 - 2\alpha_3 \\ \alpha_1 + \alpha_2 - \alpha_3 - \alpha_6 &= 2\alpha_2 - \alpha_6 = -n\alpha_6 \end{aligned} \right\} \quad (21)$$

Again, the following relations are obtained from the boundary conditions (19),

$$\begin{aligned} \alpha_2 &= \alpha_3 \\ \alpha_5 &= \alpha_6 = 0 \end{aligned} \quad (22)$$

Solving the system of linear equations (21) and (22), the following relationship are obtained,

$$\alpha_1 = 2\alpha_2 = 2\alpha_3, \alpha_4 = \alpha_5 = \alpha_6 = 0$$

by using the above relation the equation (20) reduces to the following group of transformation

$$x^* = x'e^{2\varepsilon\alpha_2}, y^* = y'e^{\varepsilon\alpha_2}, \psi^* = \psi e^{\varepsilon\alpha_2}, w^* = w', \theta^* = \theta, \varphi^* = \varphi \quad (23)$$

expanding equation (23) by Taylor's method in powers of ε and keeping terms up to the order ε , we have

$$x^* - x' = 2\varepsilon x' \alpha_2, y^* - y' = \varepsilon y' \alpha_2, \psi^* - \psi = \varepsilon \psi \alpha_2, w^* - w' = 0, \theta^* - \theta = 0, \varphi^* - \varphi = 0$$

In terms of differentials

$$\frac{dx'}{2\alpha_2 x'} = \frac{dy'}{\alpha_2 y'} = \frac{d\psi}{\alpha_2 \psi} = \frac{dw'}{0} = \frac{d\theta}{0} = \frac{d\varphi}{0} \quad (24)$$

Solving the equation (24) the following similarity variables are introduced,

$$\eta = \frac{y'}{\sqrt{x'}}, \psi = \sqrt{x'} f(\eta), w' = g_0(\eta), \theta = \theta(\eta) \text{ and } \varphi = \varphi(\eta)$$

By using the above mentioned variables, equations (15), (16), (17) and (18) becomes

$$f''' + \frac{1}{2} f f'' - M f'^2 + 2R' g_0 - \gamma f' + G_r \theta \cos \beta + G_m \varphi \cos \beta = 0 \quad (25)$$

$$g_0'' + \frac{1}{2} f g_0' - 2R' f' - \gamma g_0 - M f' g_0 = 0 \quad (26)$$

$$\frac{1}{P_r} (1 + T_c \theta + R) \theta'' + \frac{1}{P_r} T_c \theta'^2 + \frac{1}{2} f \theta' + Q \theta + E_c f''^2 = 0 \quad (27)$$

$$\frac{1}{S_c} \varphi'' + \frac{1}{2} f \varphi' - \lambda \varphi^n = 0 \quad (28)$$

The corresponding boundary conditions (19) become

$$\left. \begin{aligned} f' &= 1, f = 0, g_0 = 0, \theta = 1, \varphi = 1 \text{ at } \eta = 0 \\ f' &\rightarrow 0, g_0 \rightarrow 0, \theta \rightarrow 0, \varphi \rightarrow 0 \text{ as } \eta \rightarrow \infty \end{aligned} \right\} \quad (29)$$

where primes denote differentiation with respect to η only and the parameters are defined as

$$M = \frac{\sigma_0 B_0^2}{\rho} \text{ is the magnetic parameter,}$$

- 228 $\gamma = \frac{v^2 x'}{KU^2}$ is the porosity parameter
- 229 $R' = \frac{\Omega v x'}{U^2}$ is the rotational parameter
- 230 $G_r = \frac{g \beta_T (T_w - T_\infty) v x'}{U^3}$ is the Grashof number
- 231 $G_m = \frac{g \beta_c (C_w - C_\infty) v x'}{U^3}$ is the modified Grashof number
- 232 $T_c = c(T_w - T_\infty)$ is the thermal conductivity parameter
- 233 $P_r = \frac{v}{\alpha}$ is the Prandtl number
- 234 $R = \frac{16 \sigma_s T_\infty^3}{3 \kappa^* k_\infty}$ is the radiation parameter
- 235 $Q = \frac{Q_0 v}{\rho C_p U^2}$ is the heat source parameter
- 236 $E_c = \frac{U^2}{C_p (T_w - T_\infty)}$ is Eckert number
- 237 $S_c = \frac{v}{D_m}$ is the Schmidt number
- 238 $\lambda = \frac{k_0 (C_w - C_\infty)^{n-1} v}{U^2}$ is the reaction parameter
- 239 and n (integer) is the order of chemical reaction

240

241 **2.2 SKIN-FRICTION COEFFICIENTS, NUSSELT AND SHERWOOD NUMBER**

242

243 The physical quantities of the skin-friction coefficients, the reduced Nusselt number and
244 reduced Sherwood number are calculated respectively by the following equations,

245 $C_f (R_e)^{\frac{1}{2}} = -f''(0)$ (30)

246 $C_{g_0} (R_e)^{\frac{1}{2}} = -g'_0(0)$ (31)

247 $N_u (R_e)^{-\frac{1}{2}} = -\theta'(0)$ (32)

248 $S_h (R_e)^{-\frac{1}{2}} = -\phi'(0)$ (33)

249 where, $R_e = \frac{U x'}{v}$ is the Reynolds number.

250

251 **3. RESULTS AND DISCUSSION**

252

253 **In this paper** heat and mass transfer problem associated with laminar flow past an inclined
254 plate of a rotating system has been studied. In order to investigate the physical
255 representation of the problem, the numerical values of primary velocity, secondary velocity,
256 temperature and species concentration from equations (25), (26), (27) and (28) with the
257 boundary layer have been computed for different parameters as the magnetic parameter

(M), the rotational parameter (R'), the porosity parameter (γ), the Grashof number (G_r), the modified Grashof number (G_m), the radiation parameter (R), the Prandtl number (P_r), the Eckert number (E_c), the thermal conductivity parameter (T_c), the heat source parameter (Q), the Schmidt number (S_c), the reaction parameter (λ), the inclination angle (β) and the order of chemical reaction (n) respectively.

It is observed from the Figs. 2a and 2b that as the magnetic parameter increases, the primary and secondary velocities are decreases and increases respectively. Figs. 3a-3d represent that with the increase of rotational parameter, primary velocity decreases but secondary velocity, temperature and concentration increases.

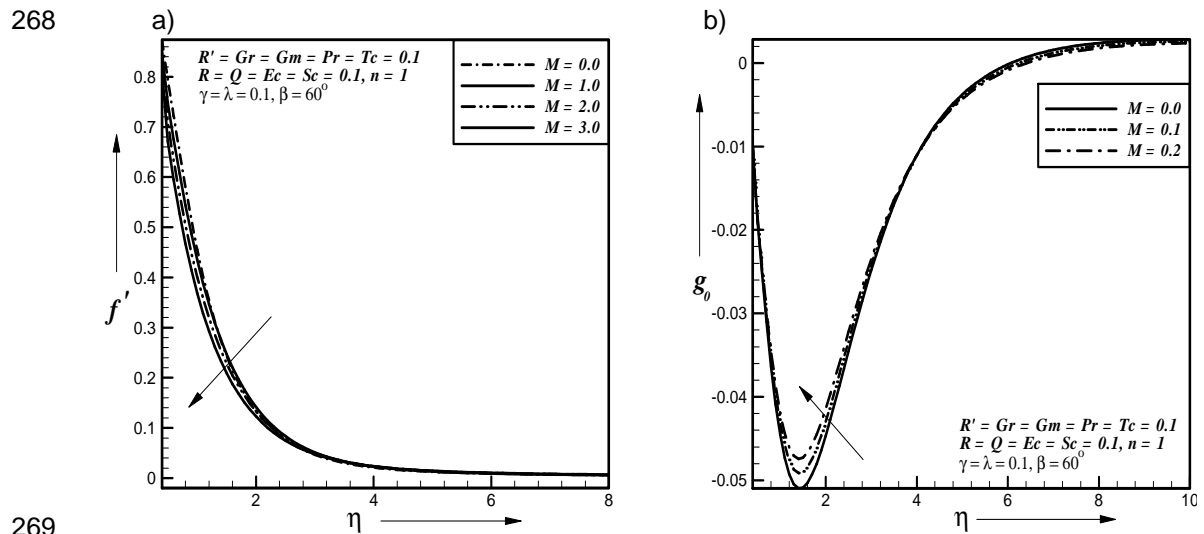
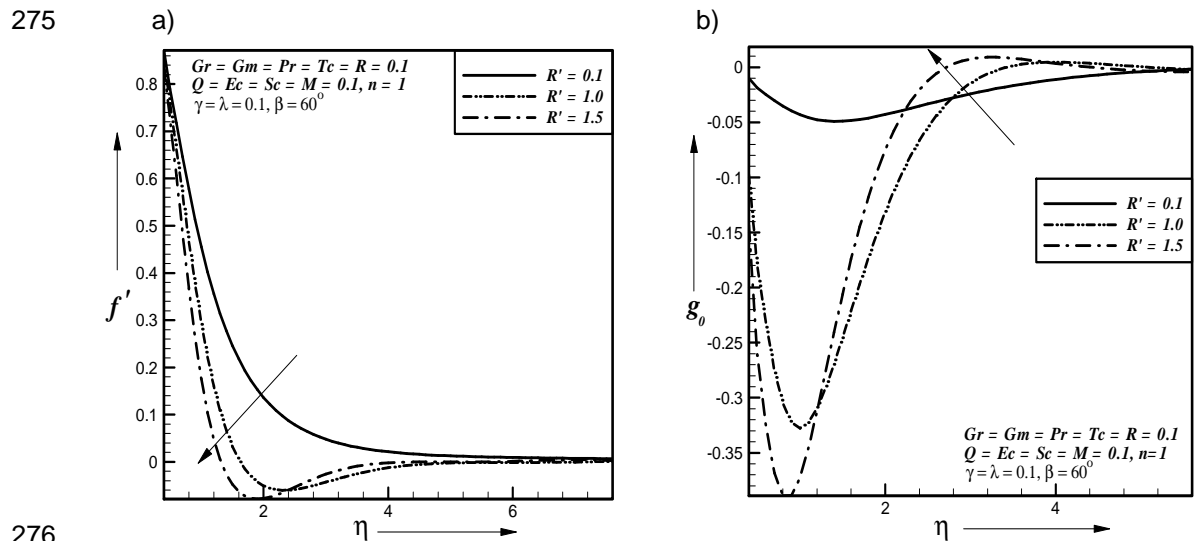
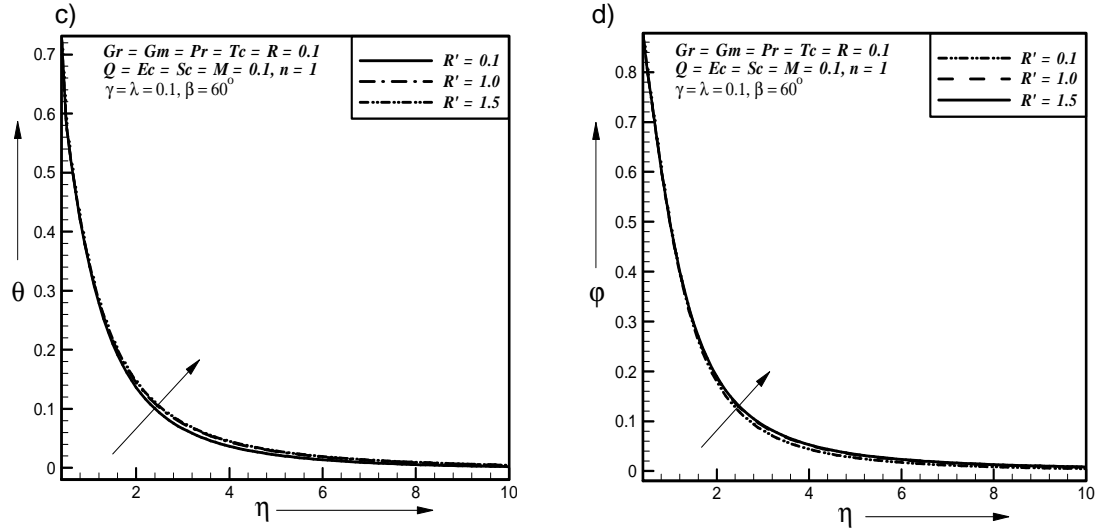


Fig. 2. Effect of magnetic parameter on a) primary velocity b) secondary velocity profiles



276
277

278



279

280

281

282

283

284

285

286

287

288

289

290

291

292

293

294

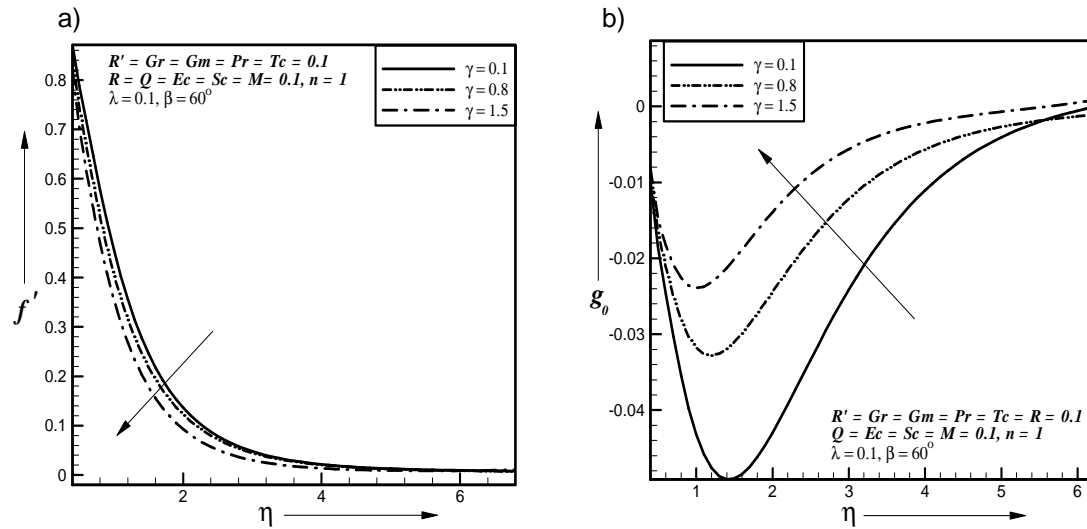
295

296

297

Fig. 3. Effect of rotational parameter on a) primary velocity b) secondary velocity c) temperature d) concentration profiles

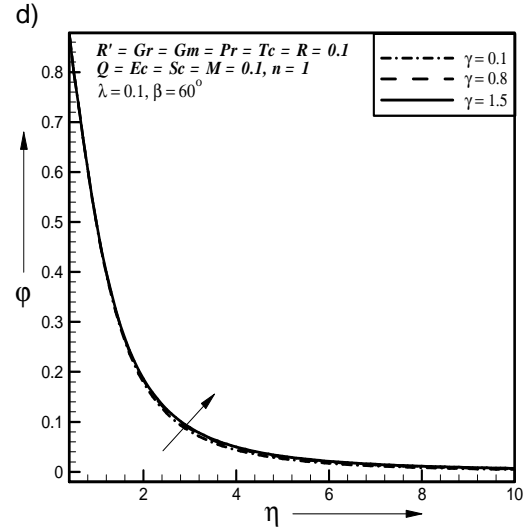
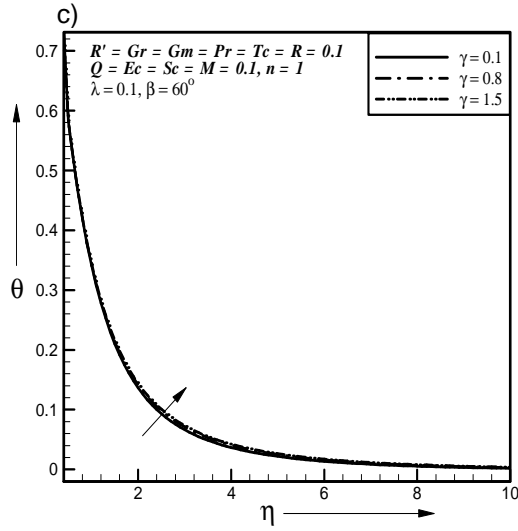
From Figs. 4a, 4b, 4c and 4d we found that with the increase of porosity parameter, primary velocity decreases but the secondary velocity, temperature and concentration is increases respectively. Figs. 5a and 5b we observed that with the increase of inclination angle primary and secondary velocity profiles decreases and increases respectively. It is observed from Figs. 6a, 6b and 6c that with the increase of Grashof number, primary velocity profile increases but secondary velocity and temperature profile decreases respectively. Figs. 7a, 7b and 7c show that with the increase of modified Grashof number, primary velocity increases but secondary velocity and concentration decreases. It is observed from Figs. 8a and 8b that with the increase of Prandtl number, primary velocity and temperature increases and decreases respectively.



298

299

300



301

302

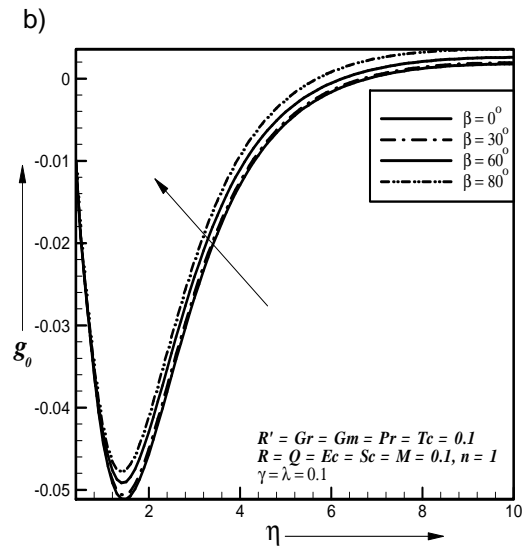
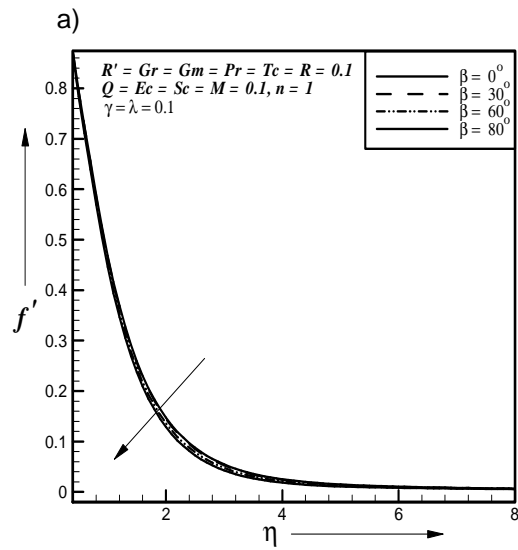
303

304

305

306

Fig. 4. Effect of porosity parameter γ on a) primary velocity b) secondary velocity c) temperature d) concentration profiles



307

308

309

310

311

312

313

314

315

316

317

318

319

320

321

Fig. 5. Effect of inclination angle on a) primary velocity b) secondary velocity profiles

322

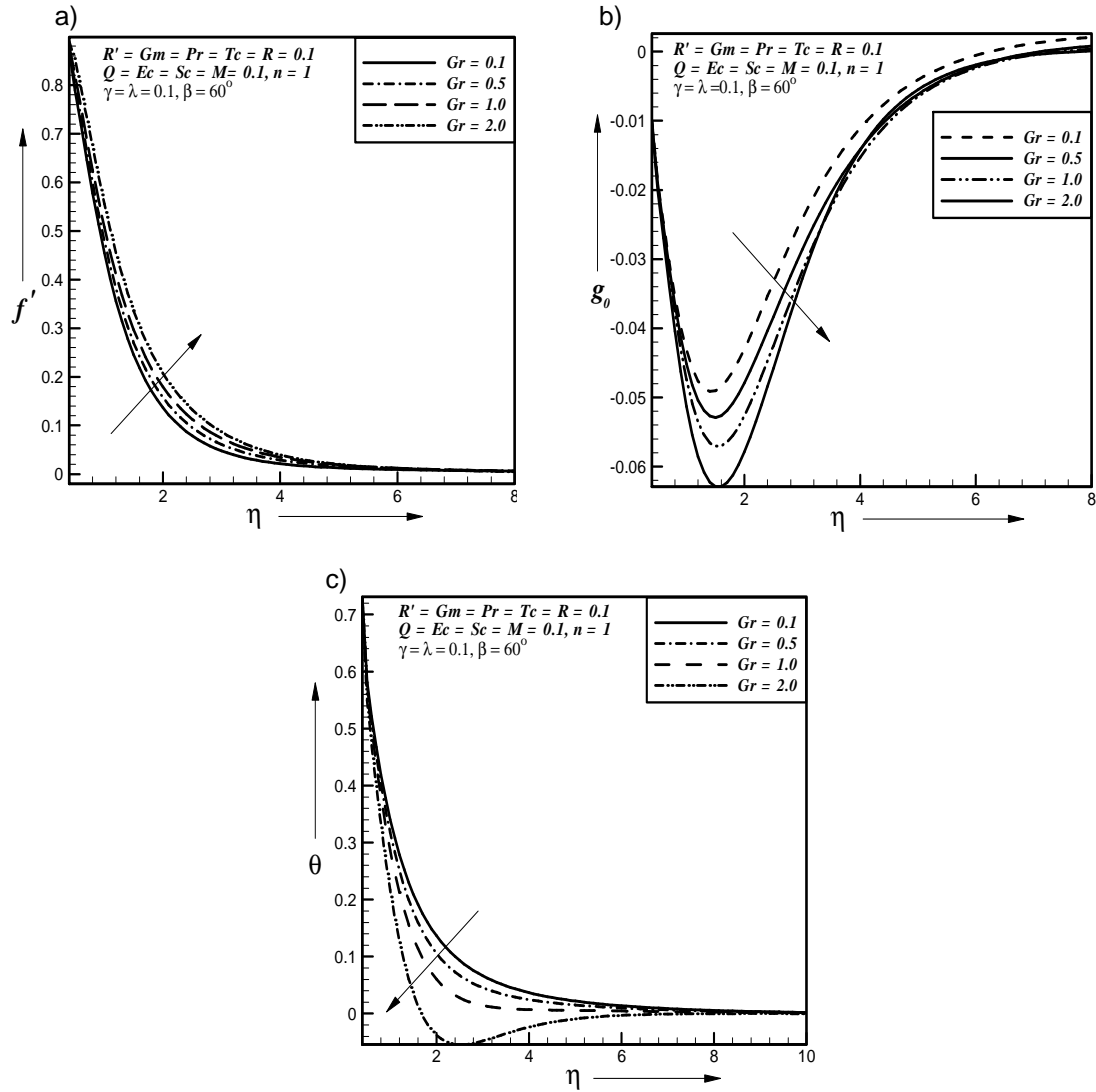
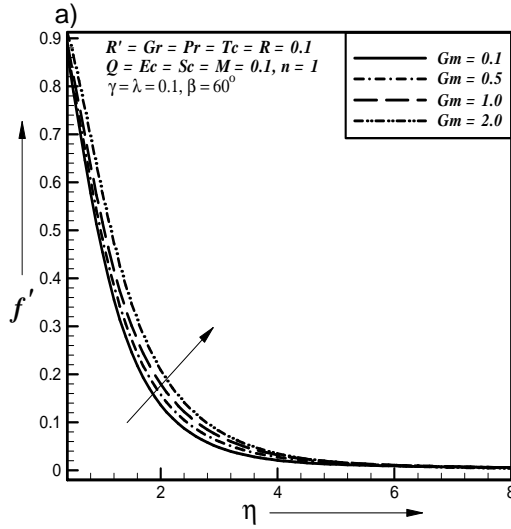
323
324
325326
327

Fig. 6. Effect of Grashof number on a) primary velocity b) secondary velocity c) temperature profiles

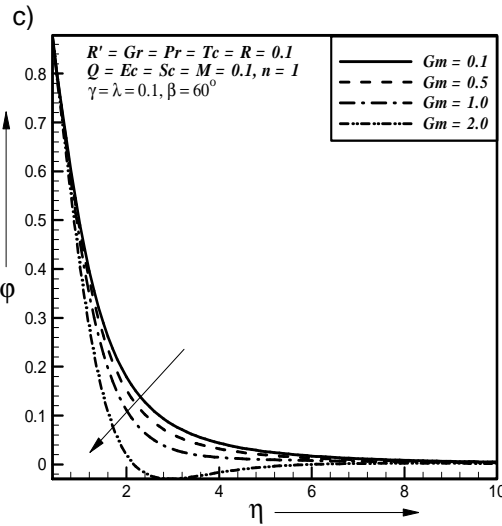
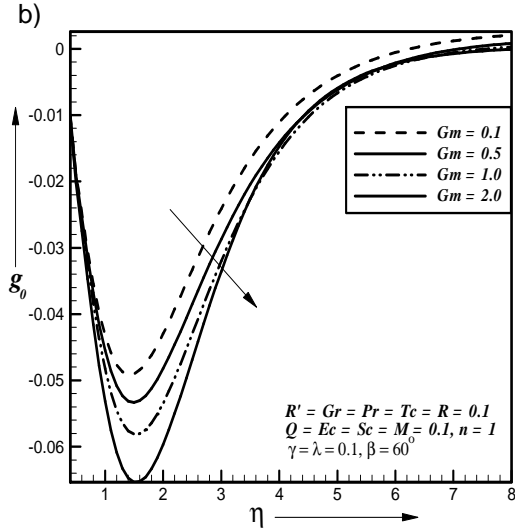
328
329
330
331
332
333
334
335
336
337
338
339
340
341
342
343
344

345



346

347



348

349

Fig. 7. Effect of modified Grashof number on a) primary velocity b) secondary velocity c) concentration profiles

350

351

352

353

354

355

356

357

358

359

360

361

362

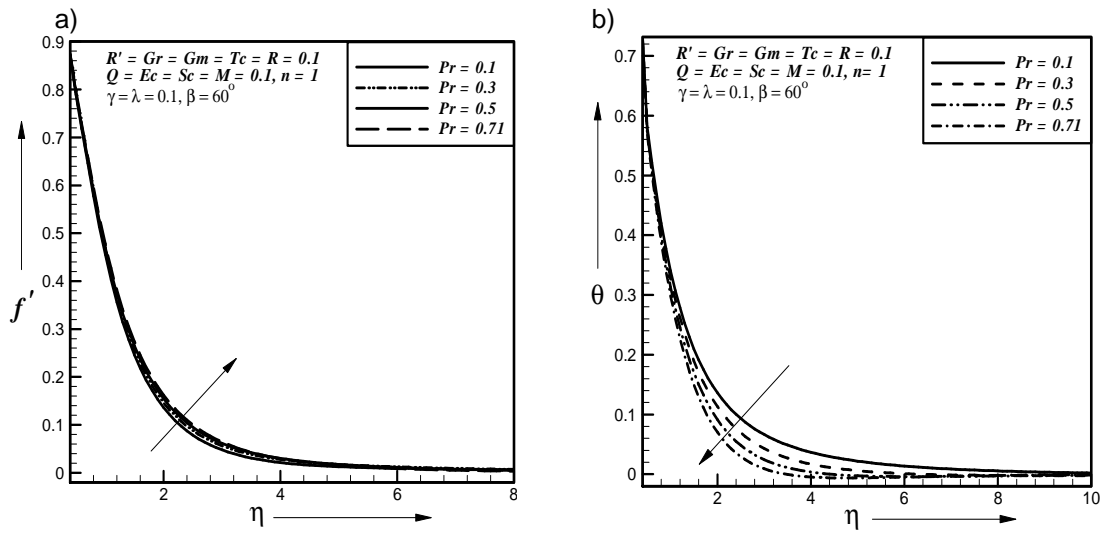
363

364

Fig. 9a displays typical profiles for primary velocity (f') for different values of Eckert number. It is observed that the primary velocity is increases with the increase of Eckert number, where other parameters have the value $M = Gr = Gm = \gamma = Pr = Tc = R = Q = R' = Sc = 0.1$, $\lambda = 0.1, \beta = 60^\circ, n = 1$.

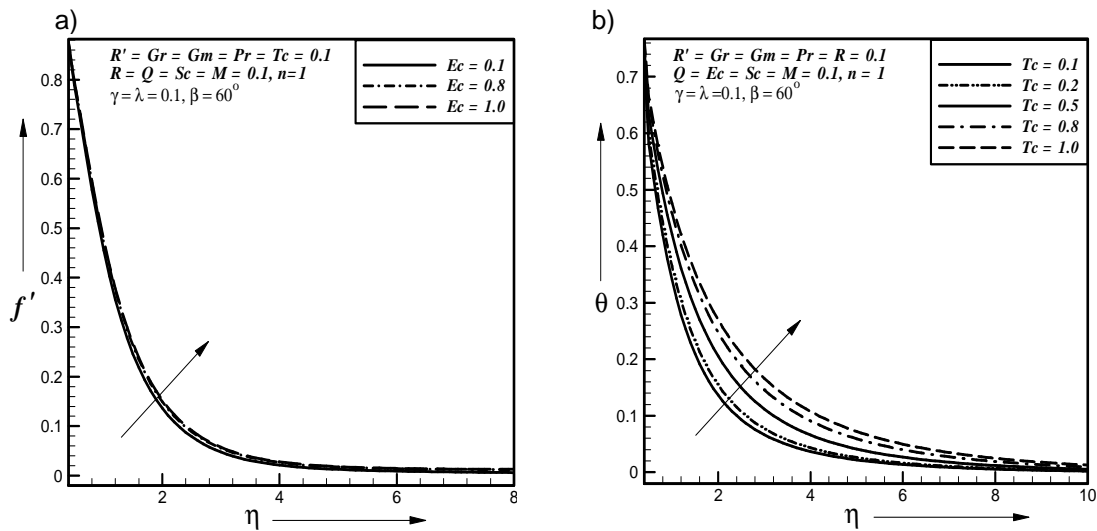
Fig. 9b displays typical profiles for temperature (θ) for different values of Thermal conductivity parameter. It is observed that the temperature is increases with the increase of Thermal conductivity parameter, where other parameters have the value $M = Gr = Gm = \gamma = Pr = 0.1, Ec = R = Q = R' = Sc = \lambda = 0.1, \beta = 60^\circ, n = 1$.

365
366



367
368
369
370
371
372

Fig. 8. Effect of Prandtl number on a) primary velocity b) temperature profiles



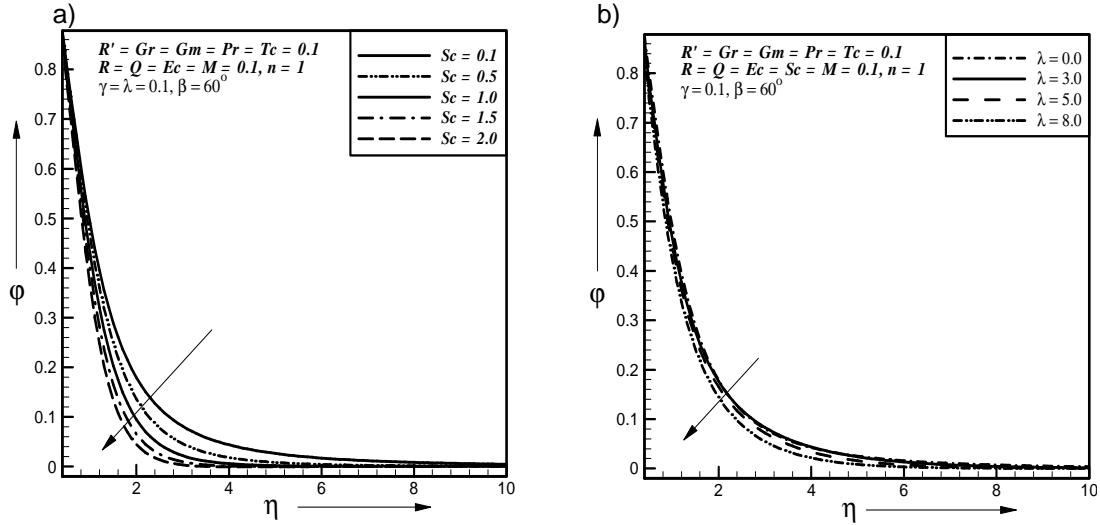
373
374
375
376
377

Fig. 9. Effect of a) Eckert number on primary velocity profiles b) thermal conductivity parameter on temperature profiles

378
379
380
381
382
383
384
385
386

Fig. 10a represents typical profiles for concentration (ϕ) for different values of Schmidt number Sc . It is observed that the concentration is decreases with the increase of Schmidt number. Fig. 10b represents no reaction ($\lambda = 0.0$) and destructive reaction ($\lambda > 0.0$) where we observed that the concentration is decreases with the increase of reaction parameter.

387



388

389

390

391

Fig. 10. Effect of a) Schmidt number on concentration profiles b) reaction parameter on concentration profiles

392

For the physical interest of the problem, the dimensionless skin-friction coefficient ($-f''$) and ($-g'_0$), the dimensionless heat transfer rate ($-\theta'$) at the plate and the dimensionless mass transfer rate ($-\phi'$) at the plate are plotted against Heat source parameter (Q) and illustrated in Figs. 11-19.

396

Figs. 11a and 11b represent the primary shear stress ($-f''$) and secondary shear stress ($-g'_0$) which are plotted against heat source parameter (Q) for different values of magnetic parameter. It is observed that the primary shear stress decreases and secondary shear stress increases with the increase of magnetic parameter, where other parameters have the value $R' = Gr = Gm = \gamma = Pr = Ec = Q = Tc = R = Sc = \lambda = 0.1$, $\beta = 60^\circ$, $n = 1$.

401

Figs. 12a and 12b represent the primary shear stress ($-f''$) and secondary shear stress ($-g'_0$) which are plotted **versus** heat source parameter (Q) for different values of rotational parameter. It is observed that the primary shear stress decreases and secondary shear stress increases with the increase of rotational parameter, where other parameters have the value.

406

407

408

409

410

411

412

413

414

415

416

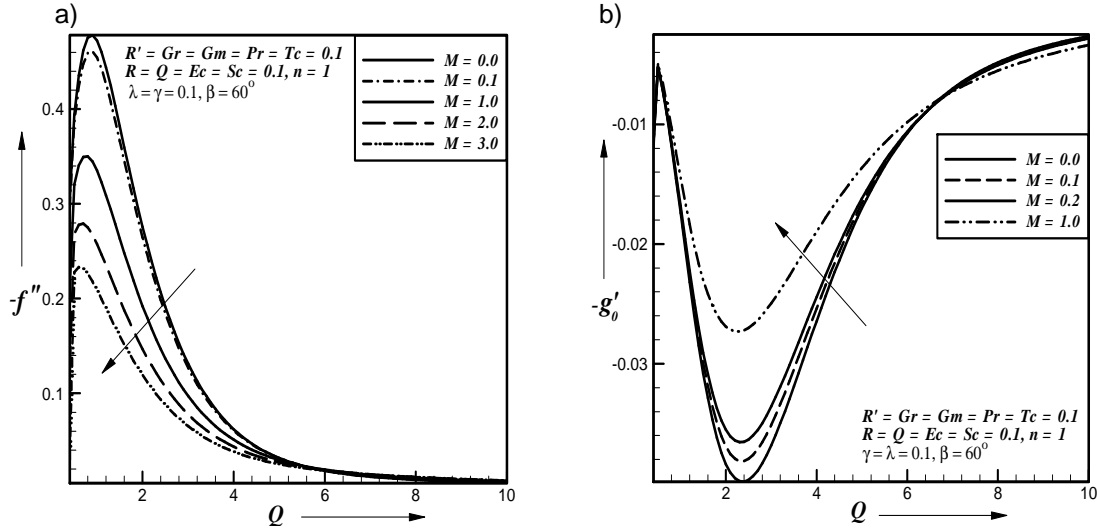
417

418

419

420

421



422

423

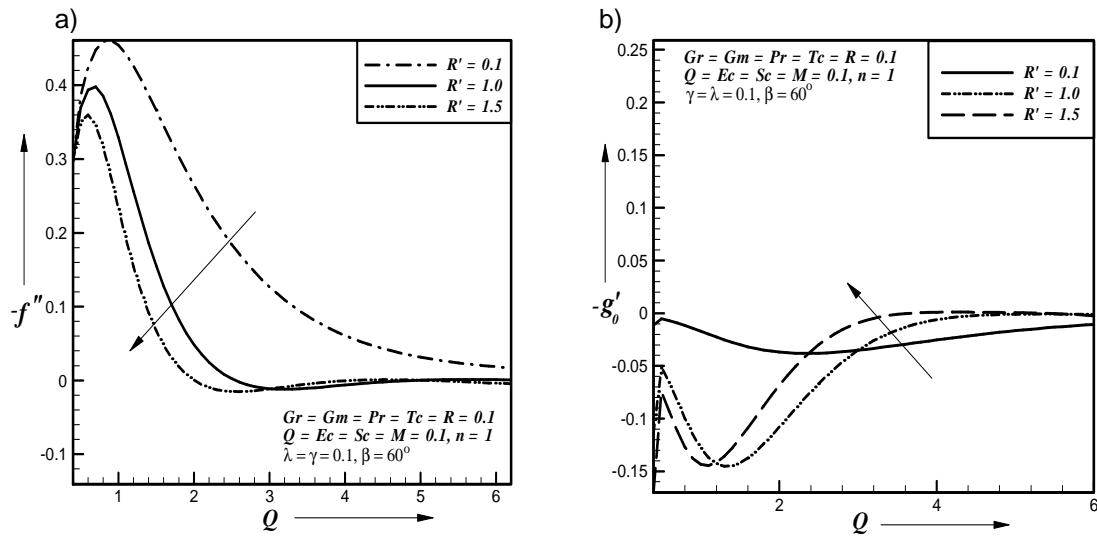
424

425

426

427

Fig. 11. Effect of magnetic parameter on a) primary shear stress b) secondary shear stress



428

429

430

431

432

433

434

435

436

437

438

439

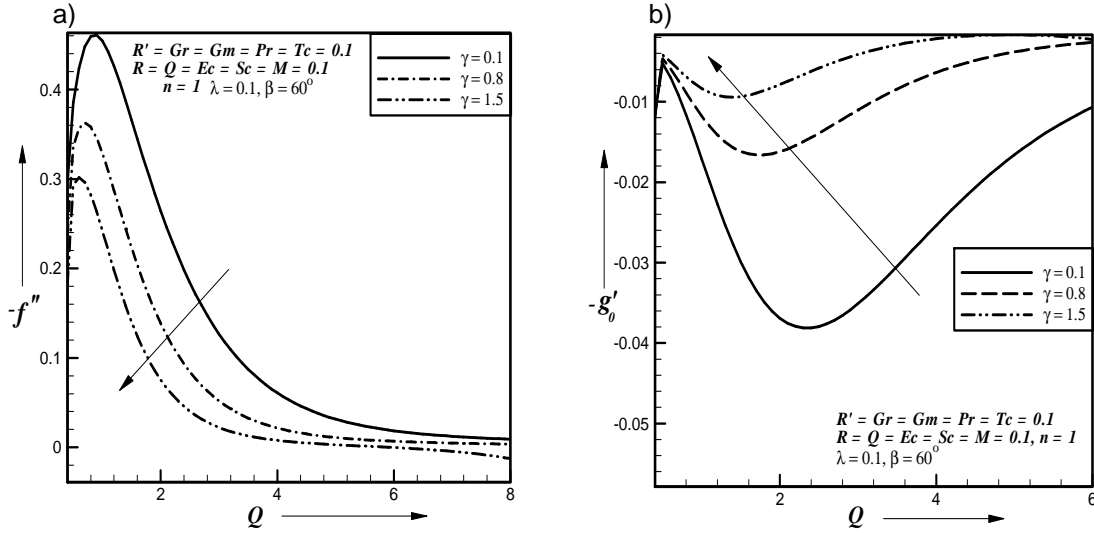
440

441

Fig. 12. Effect of rotational parameter on a) primary shear stress b) secondary shear stress

Figs. 13a and 13b represent the primary shear stress ($-f''$) and secondary shear stress ($-g'_0$) which are plotted **versus** heat source parameter (Q) for different values of porosity parameter. It is observed that the primary shear stress is decreases and secondary shear stress is increases with the increase of porosity parameter, where other parameters have the value $M = Gr = Gm = R' = Pr = Ec = Q = Tc = R = Sc = \lambda = 0.1, \beta = 60^\circ, n = 1$.

442



443

444

445

446

Fig. 13. Effect of porosity parameter on a) primary b) secondary shear stress

447

448

449

450

Fig. 14a represents the primary shear stress ($-f''$) which is plotted **versus** heat source parameter (Q) for different values of Grashof number. It is observed that the primary shear stress is increases with the increase of Grashof number, where other parameters have the value $M = \gamma = Gm = R' = Pr = Ec = Q = Tc = R = Sc = \lambda = 0.1, \beta = 60^\circ, n = 1$.

451

452

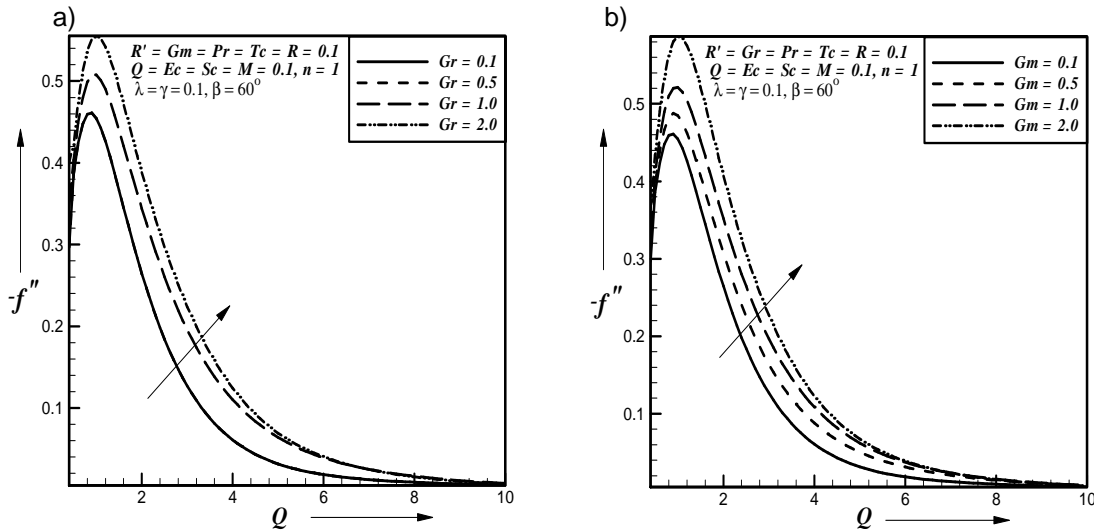
453

454

Fig. 14b represents the primary shear stress ($-f''$) which is plotted **versus** heat source parameter (Q) for different values of modified Grashof number. It is observed that the primary shear stress is increases with the increase of modified Grashof number, where other parameters have the value $M = \gamma = Gr = R' = Pr = Ec = Q = Tc = R = Sc = \lambda = 0.1, \beta = 60^\circ, n = 1$.

455

456



457

458

459

Fig. 14. Effect of a) Grashof number b) modified Grashof on primary shear stress

Fig. 15a represents the primary shear stress ($-f''$) which is plotted versus heat source parameter (Q) for different values of inclination angle. It is observed that the primary shear stress is decreases with the increase of inclination angle, where other parameters have the value $M = \gamma = Gm = Gr = R' = Pr = Ec = Q = Tc = R = Sc = \lambda = 0.1, n = 1$.

Fig. 15b represents the dimensionless heat transfer rate ($-\theta'$) which is plotted versus Heat source parameter (Q) for different values of thermal conductivity parameter. It is observed that the heat transfer rate is increases with the increase of thermal conductivity parameter, where other parameters have the value $M = \gamma = Gm = Gr = R' = Pr = Ec = Q = R = Sc = 0.1, \lambda = 0.1, \beta = 60^\circ, n = 1$.

Fig. 16a represents the dimensionless heat transfer rate ($-\theta'$) which is plotted versus heat source parameter (Q) for different values of Prandtl number. It is observes that the heat transfer rate is decreased with the increase of Prandtl number, where other parameters have the value $M = \gamma = Gm = Gr = R' = Tc = Ec = Q = R = Sc = \lambda = 0.1, \beta = 60^\circ, n = 1$.

Fig. 16b represents the dimensionless heat transfer rate ($-\theta'$) which is plotted versus Heat source parameter (Q) for different values of heat source parameter. It is observed that the heat transfer rate is increases with the increase of heat source parameter, where other parameters have the value $M = \gamma = Gm = Gr = R' = Tc = Ec = Pr = R = Sc = \lambda = 0.1, \beta = 60^\circ, n = 1$.

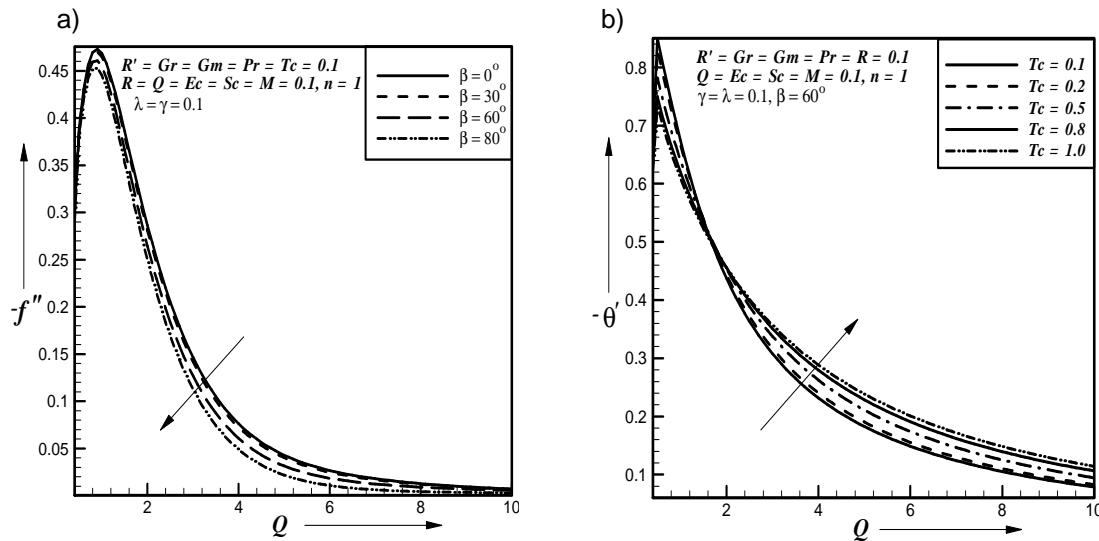
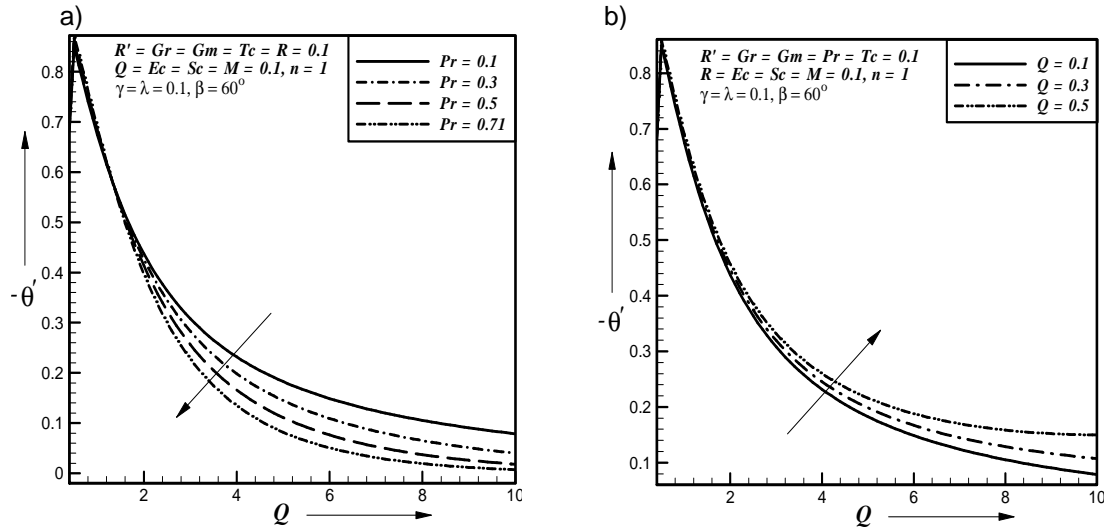


Fig. 15. Effect of a) inclination angle on primary shear stress b) thermal conductivity parameter on heat transfer rate

492



493

494

495

496

497

498

499

500

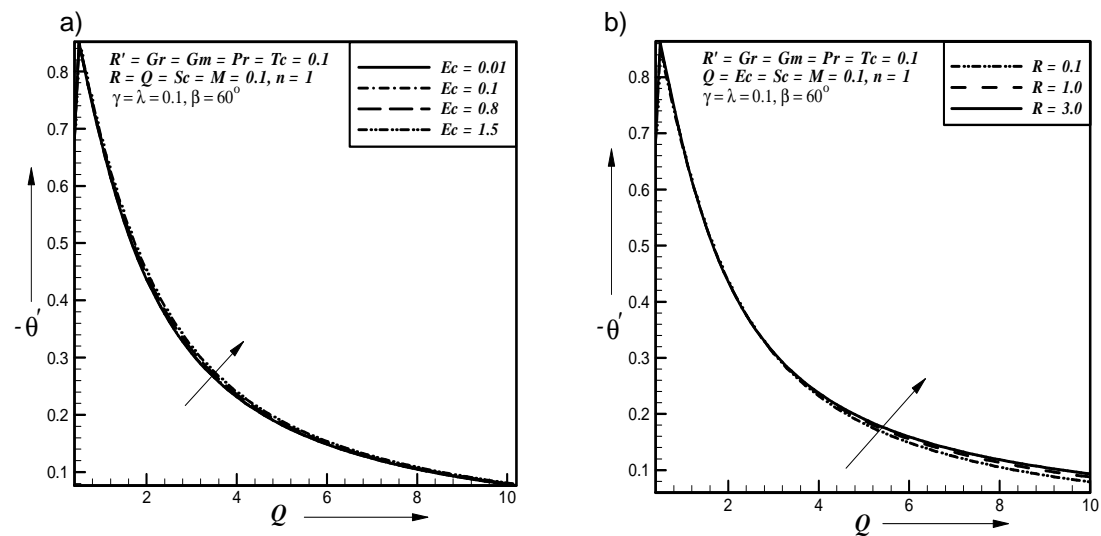
501

502

503

Fig. 16. Effect of a) Prandtl number b) heat source parameter on heat transfer rate

Fig. 17a and 17b, It is observed that the heat transfer rate increases with the increase of Eckert number and radiation parameter. Fig. 18a and Fig. 18b, show that mass transfer rate is decreases with the increase of Schmidt number and reaction parameter. Fig. 19 represents that the mass transfer rate increases with the increase of order of chemical reaction parameter.



504

505

506

507

508

509

510

511

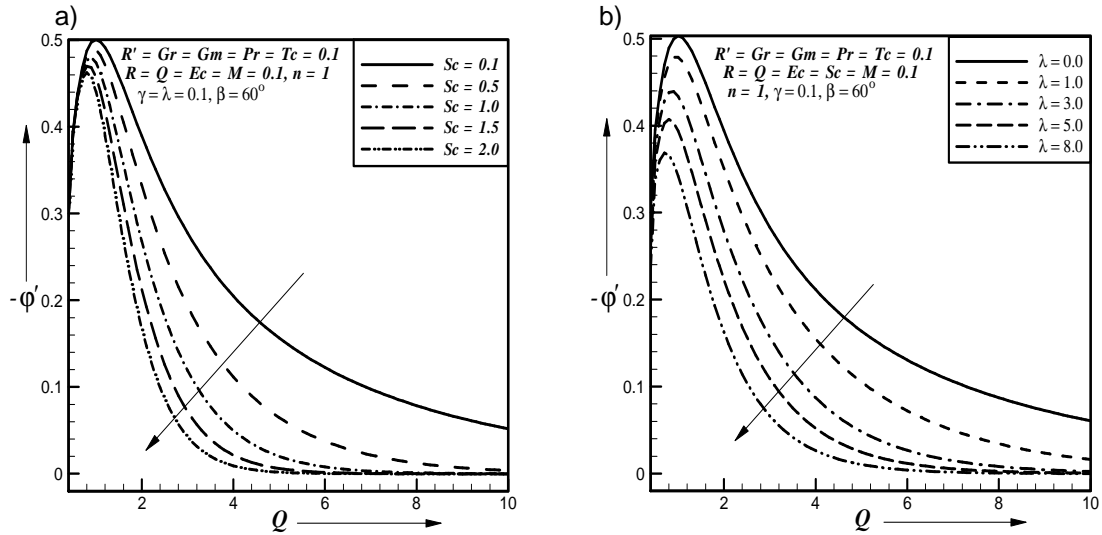
512

513

514

Fig. 17. Effect of a) Eckert number b) radiation parameter on heat transfer rate

515



516

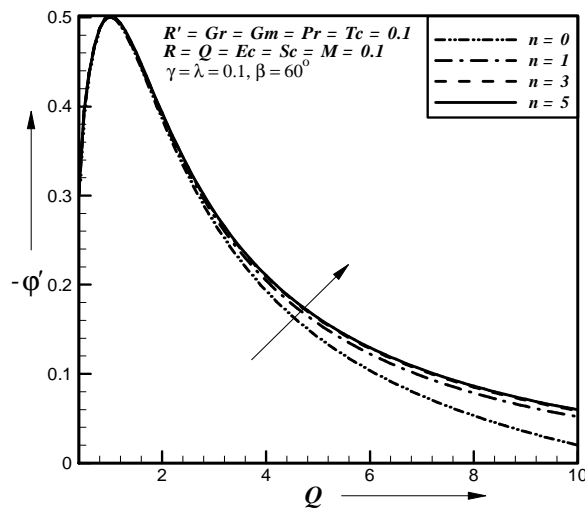
517

518

519

520

Fig. 18. Effect of a) Schmidt number b) reaction parameter on mass transfer rate



521

522

523

524

525

526

527

528

529

530

531

532

533

534

Fig. 19. Effect of order of chemical reaction on mass transfer rate

4. CONCLUSION

The important findings of the investigation from graphical representation are listed below:

The primary velocity profiles are decreases with the increase of magnetic parameter but reverse effect is found for the secondary velocity profiles. Also the primary shear stress decreases due to increase of magnetic parameter where as the reverse effect is found for secondary shear stress.

The primary velocity profiles and primary shear stress are decreases due to increase of rotational parameter where as the reverse effect is found for the secondary velocity profiles

535 and secondary shear stress. Also the temperature and concentration boundary layer
536 thickness are increases due to increase of rotational parameter.

537 The primary velocity profiles and primary shear stress are decreases due to increase of
538 permeability of the porous medium where as the reverse effect is found for the secondary
539 velocity profiles and secondary shear stress. Also the temperature and concentration
540 boundary layer thickness are increases due to increase of permeability of the porous
541 medium.

542 The primary velocity profiles and primary shear stress are decreases due to increase of
543 inclination angle where as the reverse effect is found for the secondary velocity profiles.

544 The primary velocity profiles and primary shear stress are increases due to increase of
545 Grashof number where as the reverse effect is found for the secondary velocity profiles. Also
546 the temperature boundary layer thickness is decreases due to increase of Grashof number.

547 The primary velocity profiles and primary shear stress are increases due to increase of
548 modified Grashof number where as the reverse effect is found for the secondary velocity
549 profiles. Also the concentration boundary layer thickness is decreases due to increase of
550 modified Grashof number.

551 The primary velocity profiles are increases due to increase of Prandtl number. The thermal
552 boundary layer thickness as well as the heat transfer rate at the plate is decreases as the
553 Prandtl number increases.

554 The heat transfer rate at the plate as well as the primary velocity is increases due to
555 increase of Eckert number.

556 The temperature boundary layer thickness as well as the heat transfer rate at the plate is
557 increases due to increase of thermal conductivity parameter.

558 The heat transfer rate at the plate is increases due to increase of heat source parameter.

559 The heat transfer rate at the plate is increases due to increase of radiation parameter.

560 The concentration boundary layer thickness as well as the mass transfer rate at the plate is
561 decreases due to increase of Schmidt number.

562 The concentration boundary layer thickness as well as the mass transfer rate at the plate is
563 decreases due to no reaction and destructive reaction.

564 The mass transfer rate at the plate is increases due to increase of order of chemical
565 reaction.

566 **COMPETING INTERESTS**

567
568
569 Authors have declared that no competing interests exist.
570

571 **REFERENCES**

- 572
573 1. Bluman GW, Kumei S. Symmetries and Differential Equations. Springer-verlag: New
574 York; 1989.
- 575 2. Helmy KA. MHD boundary layer equations for power law fluids with variable electric
576 conductivity. *Mechanica*. 1995;30:187-200.
- 577 3. Pakdemirli M, Yurusoy M. Similarity transformations for partial differential equations.
578 *SIAM Review*. 1998;40:96-101.
- 579 4. Kalpakides VK, Balassas KB. Symmetry groups and similarity solutions for a free
580 convective boundary-layer problem. *International Journal of Non-Linear Mechanics*.
581 2004;39:1659-1670.
582

- 583 5. Makinde OD. Free convection flow with thermal radiation and mass transfer past moving
584 vertical porous plate. *International Communications in Heat and Mass Transfer*. 2005 ;
585 32:1411-1419.
- 586 6. Seddeek MA, Salem AM. Laminar mixed convection adjacent to vertical continuously
587 stretching sheet with variable viscosity and variable thermal diffusivity. *Heat and Mass*
588 *Transfer*. 2005;41:1048-1055.
- 589 7. Ibrahim FS, Elaiw AM, Bakr AA. Effect of the chemical reaction and radiation absorption
590 on the unsteady MHD free convection flow past a semi infinite vertical permeable
591 moving plate with heat source and suction. *Communications in Nonlinear Science and*
592 *Numerical Simulation*. 2008; 13:1056-1066.
- 593 8. El-Kabeir SMM, El-Hakiem MA, Rashad. Lie group analysis of unsteady MHD three
594 dimensional dimensional by natural convection from an inclined stretching surface
595 saturated porous medium. *Journal of Computational and Applied Mathematics*.
596 2008;213:582-603.
- 597 9. Rajeswari R, Jothiram J, Nelson VK. Chemical Reaction, Heat and Mass Transfer on
598 Nonlinear MHD Boundary Layer Flow through a Vertical Porous Surface in the Presence
599 of Suction. *Applied Mathematical Sciences*. 2009;3:2469-2480.
- 600 10. Chandrakala P. Chemical Reaction Effects on MHD Flow Past An Impulsively Started
601 Semi-Infinite Vertical Plate. *International Journal of Dynamics of Fluids*. 2010;6:77-79.
- 602 11. Joneidi AA, Domairry G, Balaelahi M. Analytical treatment of MHD free convective flow
603 and mass transfer over a stretching sheet with chemical reaction. *Journal of the Taiwan*
604 *Institute of Chemical Engineers*. 2010;41: 35-43.
- 605 12. Muhaimin, Kandasamy R, Hashim I. Effect of chemical reaction, heat and mass transfer
606 on nonlinear boundary layer past a porous shrinking sheet in the presence of suction.
607 *Nuclear Engineering and Design*. 2010;240(5):933-939.
- 608 13. Rahman MM, Salahuddin KM. Study of hydromagnetic heat and mass transfer flow over
609 an inclined heated surface with variable viscosity and electric conductivity.
610 *Communications in Nonlinear Science and Numerical Simulation*. 2010;15:2073-2085.